



In situ formed depot of elastin-like polypeptide-hirudin fusion protein for long-acting antithrombotic therapy

Xue Tian^a, Mingxing Feng^a, Xinwei Wei^b, Cheng Cheng^a, Kaixin He^b , Tianyue Jiang^{a,1} , Bingfang He^{a,1}, and Zhen Gu^{b,c,d,e,1}

Edited by David Weitz, Harvard University, Cambridge, MA; received August 22, 2023; accepted January 30, 2024

Thrombosis, induced by abnormal coagulation or fibrinolytic systems, is the most common pathology associated with many life-threatening cardio-cerebrovascular diseases. However, first-line anticoagulant drugs suffer from rapid drug elimination and risk of hemorrhagic complications. Here, we developed an *in situ* formed depot of elastin-like polypeptide (ELP)-hirudin fusion protein with a prodrug-like feature for long-term antithrombotic therapy. Highly secretory expression of the fusion protein was achieved with the assistance of the Ffu312 tag. Integration of hirudin, ELP, and responsive moiety can customize fusion proteins with properties of adjustable *in vivo* retention and controllable recovery of drug bioactivity. After subcutaneous injection, the fusion protein can form a reservoir through temperature-induced coacervation of ELP and slowly diffuse into the blood circulation. The biological activity of hirudin is shielded due to the N-terminal modification, while the activated key proteases upon thrombus occurrence trigger the cleavage of fusion protein together with the release of hirudin, which has antithrombotic activity to counteract thrombosis. We substantiated that the optimized fusion protein produced long-term antithrombotic effects without the risk of bleeding in multiple animal thrombosis models.

drug delivery | elastin-like polypeptide | antithrombotic therapy | bioresponsive materials

Cardio-cerebrovascular diseases are the main contributor to the global medical burden, with morbidity and mortality ranking first among non-communicable diseases worldwide (1–3). Thrombosis is the most common underlying pathology of cardio-cerebrovascular disorders (4–6). The formation of thrombus caused by dysregulation of the hemostasis system can block the blood vessels (7, 8). Once a clot occludes at a critical location, it can induce life-threatening symptoms, including ischemic stroke, myocardial infarction, and pulmonary embolism (9–12).

Anticoagulant drugs as the first line of defense have been exploited to inhibit the formation and extension of thrombus (13, 14). Heparin is the most routinely applied anti-coagulant but suffers from a risk of bleeding and thrombocytopenia in clinical settings (15). Heparin-induced thrombocytopenia is an immune-associated adverse effect that can cause severe thrombotic complications (16, 17). Hirudin, a polypeptide extracted from the leech, has been developed as a potent alternative anticoagulant (18). Distinct from heparin, there is no interaction between hirudin and platelets to induce any thrombocytopenia (19). The US Food and Drug Administration has approved recombinant hirudin and its derivates, including lepirudin, desirudin, and bivalirudin for antithrombotic therapy (13). However, the short half-life of recombinant hirudin necessitates frequent administration. For example, the clinical application of desirudin is subcutaneously injected at an initial dose before surgery, followed by a maintenance dose twice a day for deep vein thrombosis prophylaxis (20). Thus, long-acting formulations with a low administration frequency are highly desired.

Here, we reported a safe and long-acting elastin-like polypeptide (ELP)-hirudin fusion protein for antithrombotic therapy (Fig. 1A). Through conjugating hirudin, ELP, and responsive moiety via genetic engineering, a customized fusion protein was obtained with the characteristics of *in situ* depot formation, tunable *in vivo* retention and controllable recovery of bioactivity. ELPs are thermoresponsive biopolymers typically composed of pentapeptide Val-Pro-Gly-Xaa-Gly (VPGXG) repetitive unit derived from tropoelastin (21, 22). The intrinsic properties of reversible soluble-insoluble phase transition, as well as excellent biodegradability and biocompatibility (23–26), make ELP a promising fusion partner. In this study, the number of repeat unit VPGXG (X is Val and His in the ratio of 1:4) of ELP was adjusted from 20 to 160 to regulate the phase transition temperature (T_g) and *in vivo* retention time of the fusion protein. Among them, the fusion protein with 120 repeat units (ELP120) exhibited optimal long-term performance.

Significance

Anticoagulant drugs used in clinics for the prevention of thrombosis are subject to frequent administration and risk of bleeding complications. In this study, we present a long-acting and safe antithrombotic treatment strategy by integrating hirudin, elastin-like peptide, and responsive moiety through genetic engineering. The customized fusion protein can form an *in situ* depot for sustained release. Importantly, the fusion protein remains inactive in the circulation, while the proteases activated during thrombosis can degrade the fusion protein to generate active hirudin, potentiating antithrombotic efficacy against thrombosis.

Author affiliations: ^aSchool of Pharmaceutical Sciences, Nanjing Tech University, Nanjing 211816, China;

^bKey Laboratory of Advanced Drug Delivery Systems of Zhejiang Province, National Key Laboratory of Advanced Drug Delivery and Release Systems, College of Pharmaceutical Sciences, Zhejiang University, Hangzhou 310058, China; ^cJinhua Institute of Zhejiang University, Jinhua 321299, China; ^dDepartment of General Surgery, Sir Run Shaw Hospital, School of Medicine, Zhejiang University, Hangzhou 310016, China; and ^eLiangzhu Laboratory, Hangzhou 311121, China

Author contributions: T.J., B.H., and Z.G. designed research; X.T. and M.F. performed research; K.H. contributed new reagents/analytic tools; X.T., C.C., K.H., T.J., and Z.G. analyzed data; and X.T., M.F., X.W., C.C., T.J., and B.H. wrote the paper.

Competing interest statement: Z.G. is a scientific co-founder of Zonomics Inc., ZCapsule Inc., and μ Zen Pharma Co., Ltd. The other authors declare no conflicting interests.

This article is a PNAS Direct Submission.

Copyright © 2024 the Author(s). Published by PNAS. This article is distributed under Creative Commons Attribution-NonCommercial-NoDerivatives License 4.0 (CC BY-NC-ND).

¹To whom correspondence may be addressed. Email: tjiang@njtech.edu.cn, bingfanghe@njtech.edu.cn, or guzhen@zju.edu.cn.

This article contains supporting information online at <https://www.pnas.org/lookup/suppl/doi:10.1073/pnas.2314349121/-DCSupplemental>.

Published March 5, 2024.

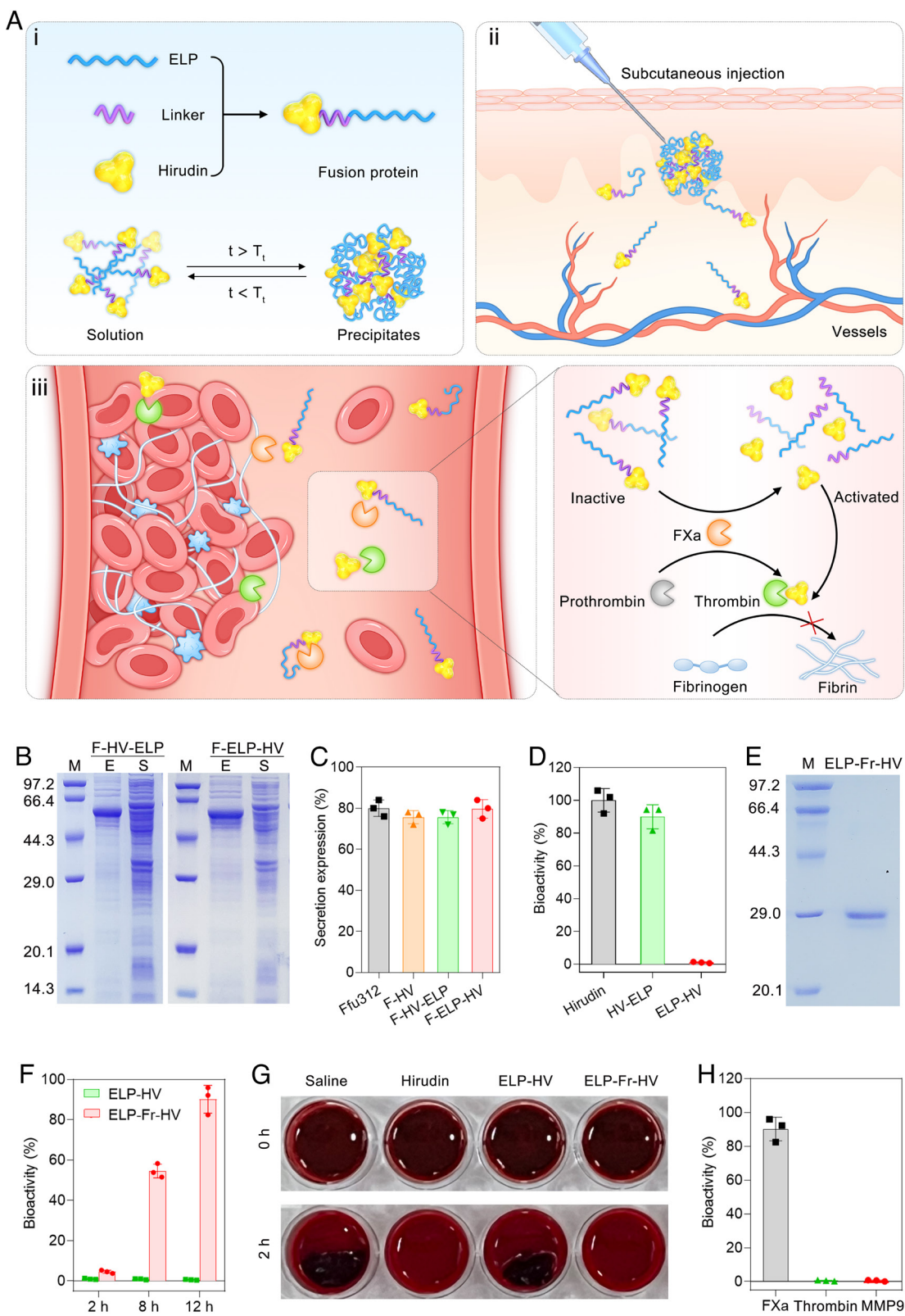


Fig. 1. (A) Schematic illustration of in situ formed depot of ELP-Fr-HV fusion protein for long-acting antithrombotic therapy. (i) Construction of fusion protein with reversible phase transition property. (ii) In situ formed depot and sustained release of fusion protein. (iii) The FXa-responsive bioactivity recovery of fusion protein during thrombosis. (B–H) Expression, purification, and in vitro anticoagulant activity of fusion proteins. (B) SDS-PAGE analysis of expression of F-HV-ELP and F-ELP-HV. M: protein marker, E: excretion to the culture medium, S: supernatant of cell lysis. (C) Secretory expression percentage of target proteins in total secretion. Data are presented as the mean \pm SD, $n = 3$ independent experiments. (D) Bioactivity of hirudin, HV-ELP, and ELP-HV. Data are presented as the mean \pm SD, $n = 3$ independent experiments. (E) SDS-PAGE analysis of purified ELP-Fr-HV. (F) Bioactivity of ELP-Fr-HV and ELP-HV after incubation with FXa for 2 h, 8 h, and 12 h. Data are presented as the mean \pm SD, $n = 3$ independent experiments. (G) Whole-blood incubation with hirudin, ELP-HV, and ELP-Fr-HV for 2 h. (H) Bioactivity of ELP-Fr-HV after incubation with FXa, thrombin, and MMP9 for 12 h. Data are presented as the mean \pm SD, $n = 3$ independent experiments.

To further minimize the potential risk of bleeding, the lesion-responsive degradable moiety was introduced into the fusion protein for precise bioactivity regulation. In the pathological condition of thrombosis, several crucial proteases (27, 28), such as FXa and thrombin, are activated, which can be leveraged as potential biosignal stimuli for on-demand drug release (29–32). We fused FXa/thrombin-responsive moiety tetrapeptide between ELP and recombinant hirudin variant 1 (HV) for the construction of fusion proteins, ELP-Fr-HV and ELP-Tr-HV, respectively, both of which exhibited robust and specific anticoagulation activity recovery. After subcutaneous injection, the fusion protein formed a reservoir through temperature-triggered coacervation of ELP and was slowly released into the blood. The biological activity of hirudin was closed off due to the N-terminal modification, while the elevation of associated proteases upon thrombus occurrence resulted in the degradation of fusion proteins together with the production of hirudin, which generated antithrombotic activity to counteract thrombosis. We verified that ELP120-Fr-HV after subcutaneous administration produced long-term antithrombotic effects without bleeding risk in several animal thrombosis models.

Results

Design of Fusion Proteins. The Ffu312 tag, a truncation from β -fructofuranosidase (33, 34), was used for the efficient secretory expression of various target proteins (*SI Appendix*, Fig. S1). The Ffu312 tag (molecular weight (MW) = 35.3 kDa) was first fused to the anticoagulant drug hirudin. As examined by the sodium dodecyl sulfate-polyacrylamide gel electrophoresis (SDS-PAGE) analysis, in comparison to barely any visible band of hirudin (MW = 7 kDa) at the expected position in either soluble form or inclusion body (*SI Appendix*, Fig. S2), a large amount of the fusion protein, Ffu312-tagged hirudin (F-HV, MW = 42.8 kDa) was observed in the culture medium (*SI Appendix*, Fig. S3), indicating the highly efficient secretory expression of F-HV mediated by the Ffu312 tag. The RNA structure analysis of the secondary structure of the translation initiation region of F-HV presented more exposure of the start codon and increased minimum free energy (from -14.4 to -9.9 kcal/mol) than that of hirudin (*SI Appendix*, Fig. S4), suggesting that the introduction of Ffu312 tag protects hirudin with small molecule weight from protease degradation and also makes the expression of hirudin easy to implement. After the enterokinase (EK) digestion of F-HV to remove the Ffu312 tag followed by anion exchange chromatography purification, the purified hirudin was obtained with the bioactivity of ~15,000 ATU/mg as determined by the antithrombin assay (*SI Appendix*, Fig. S5).

Next, we introduced the biopolymer ELP derived from the human tropoelastin into the fusion protein. To investigate the impact of fusion position on the bioactivity of hirudin, ELP composed of 40 repetitive units was conjugated to the C-terminus and N-terminus of hirudin to obtain HV-ELP and ELP-HV, respectively. The significant extracellular expression levels of the Ffu312-tagged HV-ELP (F-HV-ELP, MW = 61 kDa) and ELP-HV (F-ELP-HV, MW = 61 kDa) were observed (Fig. 1B), confirming that the Ffu312 tag remained high secretory expression capability with a yield of ~300 mg/L even when it was applied to large passenger proteins. Through grayscale scanning analysis, the secretory expression of each target protein was all higher than 75% of the total secretion (Fig. 1C). Inverse transition cycling (ITC) (35), a facile chromatography-free purification process (*SI Appendix*, Fig. S6), was used to purify HV-ELP and ELP-HV after removal of the Ffu312 tag by the EK digestion (*SI Appendix*, Fig. S7). Following that, we measured the anticoagulant effect of HV-ELP and ELP-HV. The bioactivity of

HV-ELP was ~90% of free hirudin, while ELP-HV exhibited almost no anticoagulation effect (Fig. 1D). It has been reported that the anticoagulant function of hirudin is attributed to the insertion of the N-terminus of hirudin into the active site canyon of thrombin (36). Therefore, the N-terminal modification can impede the affinity between hirudin and the active center of thrombin, which hinders the antithrombin activity of hirudin.

The intense influence of the N-terminal capping on the bioactivity of hirudin lays a foundation for the design of prodrug-like fusion proteins. The introduction of a thrombosis-associated protease-degradable linker between the C-terminus of ELP and the N-terminus of hirudin allows the “off-on” switching of the antithrombin activity of the fusion protein. We hypothesized that the N-terminal modification shielded the biological activity of hirudin in blood circulation, while the crucial proteases involved in clot formation could catalyze the degradation of the responsive linker of the fusion protein to activate the antithrombin activity. The hirudin with an extra methionine residue at the N-terminus also had no antithrombin activity (*SI Appendix*, Fig. S8), suggesting that only one amino acid residue of the linker at the N-terminal of hirudin can have a vast impact on its biological activity. Different from metalloproteinases and aspartic proteases that require specific residues on both sides of the cleavage site (37, 38), serine protease FXa serves as a potential biosignal stimulus, since FXa can hydrolyze the Ile-Glu-Gly-Arg (IEGR) motif from the C-terminus of arginine to release hirudin with no residue. Moreover, FXa, as a central enzyme in the coagulation pathway, is activated upon thrombus occurrence. Therefore, we fused the IEGR peptide linker into ELP-HV to construct the FXa-responsive fusion protein, ELP-Fr-HV.

To prove the prodrug-like feature, we harvested the purified ELP-Fr-HV by the same method as ELP-HV (Fig. 1E) and monitored its FXa-responsive activity recovery using the antithrombin assay. The addition of FXa resulted in the rapid bioactivity recovery of ELP-Fr-HV, while non-responsive ELP-HV did not show any noticeable bioactivity before and after treatment (Fig. 1F). The bioactivity recovery of ELP-Fr-HV was further validated by applying ELP-Fr-HV to the fresh whole blood. In the presence of ELP-Fr-HV or hirudin, the blood was prevented from clotting within the studied period of 2 h, whereas the blood rapidly coagulated in the saline and ELP-HV treated groups (Fig. 1G). The responsive specificity of ELP-Fr-HV to FXa was assessed by treating ELP-Fr-HV with other proteases, thrombin and matrix metalloproteinase-9 (MMP9). No bioactivity recovery of ELP-Fr-HV was detected when co-incubated with thrombin or MMP9 (Fig. 1H). These data suggest that FXa can specifically recognize and cleave the responsive motif of ELP-Fr-HV, releasing hirudin to produce an antithrombin effect. Furthermore, to verify the adaptability of the responsive motif, we constructed the thrombin-responsive fusion protein, ELP-Tr-HV by substituting the FXa-recognized IEGR motif with the thrombin-recognized Leu-Thr-Pro-Arg motif (*SI Appendix*, Fig. S9A). Thrombin, another pivotal biosignal in the pathogenesis of thrombosis also belongs to serine protease (39). Likewise, in the fresh whole blood study, the blood was prevented from clotting by ELP-Tr-HV (*SI Appendix*, Fig. S9B), suggesting that the responsiveness of fusion protein is tunable via fusing various degradable motifs in response to the corresponding proteases.

Series of Fusion Proteins with Adjustable T_t . To screen out ELP-Fr-HV with appropriate T_t for optimal *in vivo* performance, a series of ELPs with lengths of 20 to 160 repeats were designed to construct the fusion protein ELP_n-Fr-HVs. Significant extracellular expression of Ffu312-tagged ELP_n-Fr-HVs (F-ELP_n-Fr-HVs, n = 20, 40, 80, 120, 160; MW = 52.6, 61.4, 79.0, 96.6, 114.2

kDa) was observed by SDS-PAGE analysis (Fig. 2A). After EK cleavage and repeated ITC purification, we obtained a series of ELPn-Fr-HVs with high purities (Fig. 2B). As evidenced by the antithrombin assay, the bioactivity of ELPn-Fr-HVs containing different ELP lengths was almost completely blocked, which was all rapidly recovered after the addition of FXa (Fig. 2C). Subsequently, we monitored the thermoresponsive phase transition behaviors of the ELPn-Fr-HV proteins by turbidity measurement from 4 °C to 80 °C (Fig. 2D). All the fusion proteins displayed distinct thermally reversible phase transitions, as the optical density increased sharply with the increasing temperature. The more repetitive units of the ELP segment, the lower T_t of ELPn-Fr-HV. At the concentration of 20 μM, the T_t of ELP80-Fr-HV, ELP120-Fr-HV, and ELP160-Fr-HV were 35 °C, 26 °C, and 22 °C, respectively, while the T_t of ELP20-Fr-HV and ELP40-Fr-HV were 62 °C and 44 °C, respectively, suggesting that ELP80-Fr-HV, ELP120-Fr-HV, and ELP160-Fr-HV have the potential to form depot at body temperature. Meanwhile, the compounds would be released from the subcutaneous depots by peripheral dilution, since T_t increased with the dilution of fusion proteins (Fig. 2E).

Furthermore, dynamic light scattering data showed that each ELPn-Fr-HV exhibited a sharp increase in size induced by the stepwise rise of temperature (Fig. 2F). The temperature range of size variation was generally consistent with the T_t measured by the turbidity method. The optical images of ELPn-Fr-HVs at

different temperatures were observed to show the appearance changes of fusion proteins. All ELPn-Fr-HVs were clear after incubation at 10 °C for 24 h (Fig. 2G). In contrast, after incubation at 37 °C for 5 min, ELP80-Fr-HV, ELP120-Fr-HV, and ELP160-Fr-HV transformed into white suspensions, while ELP20-Fr-HV and ELP40-Fr-HV remained clear. The release profiles of rhodamine-labeled ELPn-Fr-HVs (Rho-ELPn-Fr-HVs) were evaluated at 37 °C. Then, ~90% of rhodamine-labeled hirudin (Rho-HV) was rapidly released within 1 h (Fig. 2H). In comparison, all fusion proteins exhibited sustainable release, especially Rho-ELP120-Fr-HV and Rho-ELP160-Fr-HV.

In Vivo Retention Time. Next, we investigated the in vivo retention behaviors of ELPn-Fr-HVs with variable T_t . Cyanine7-labeled ELPn-Fr-HVs (Cy7-ELPn-Fr-HVs) were injected subcutaneously in mice and imaged for up to 5 d using the in vivo imaging system. Compared to the rapid signal attenuation of cyanine7-labeled hirudin, which is ascribed to the rapid diffusion of hirudin into circulation, the introduction of ELP with different lengths all prolonged the subcutaneous residue time of hirudin to different extents (Fig. 3A), partly due to the increase of molecular weight. Notably, substantially large depots were observed after the subcutaneous injection of Cy7-ELP120-Fr-HV and Cy7-ELP160-Fr-HV, and the fluorescence signals of Cy7-ELP120-Fr-HV and Cy7-ELP160-Fr-HV were still visible within 5 d after a single

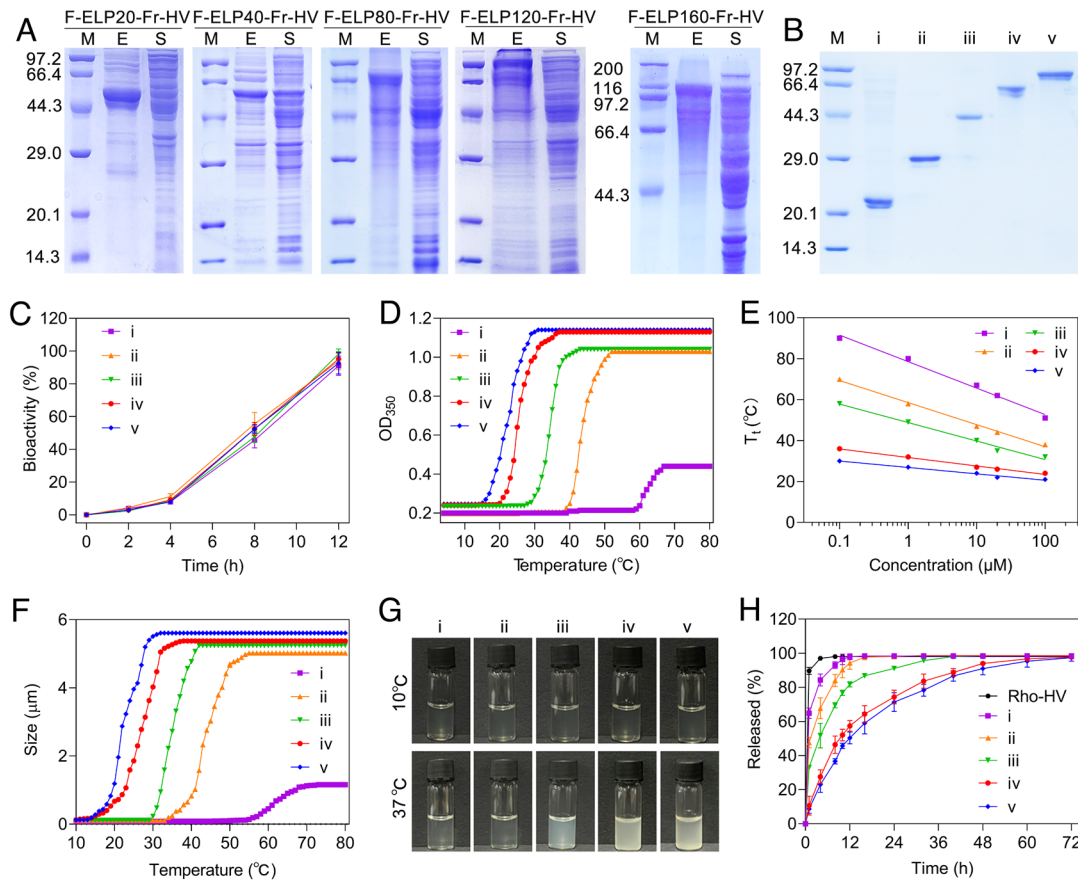


Fig. 2. Expression, purification, and in vitro characterizations of ELPn-Fr-HVs with different lengths of ELP. (A) SDS-PAGE analysis of expression of F-ELPn-Fr-HVs ($n = 20, 40, 80, 120, 160$). M: protein marker; E: excretion to the culture medium; S: supernatant of cell lysis. (B–G) In vitro characterizations of ELPn-Fr-HVs. i: ELP20-Fr-HV; ii: ELP40-Fr-HV; iii: ELP80-Fr-HV; iv: ELP120-Fr-HV; v: ELP160-Fr-HV. (B) SDS-PAGE analysis of purified ELPn-Fr-HVs. (C) Changes in the bioactivity of ELPn-Fr-HVs after incubation with FXa over time. Data are presented as the mean \pm SD, $n = 3$ independent experiments. (D) Turbidity (OD350) versus temperature of ELPn-Fr-HVs at 20 μM in PBS. (E) T_t versus concentration of ELPn-Fr-HVs. (F) Size versus temperature of ELPn-Fr-HVs at 20 μM in PBS. (G) Optical images of 20 μM ELPn-Fr-HVs at 10 °C and 37 °C. (H) Release profiles of Rho-ELPn-Fr-HVs at 37 °C. i: Rho-ELP20-Fr-HV; ii: Rho-ELP40-Fr-HV; iii: Rho-ELP80-Fr-HV; iv: Rho-ELP120-Fr-HV; v: Rho-ELP160-Fr-HV. Data are presented as the mean \pm SD, $n = 3$ independent experiments.

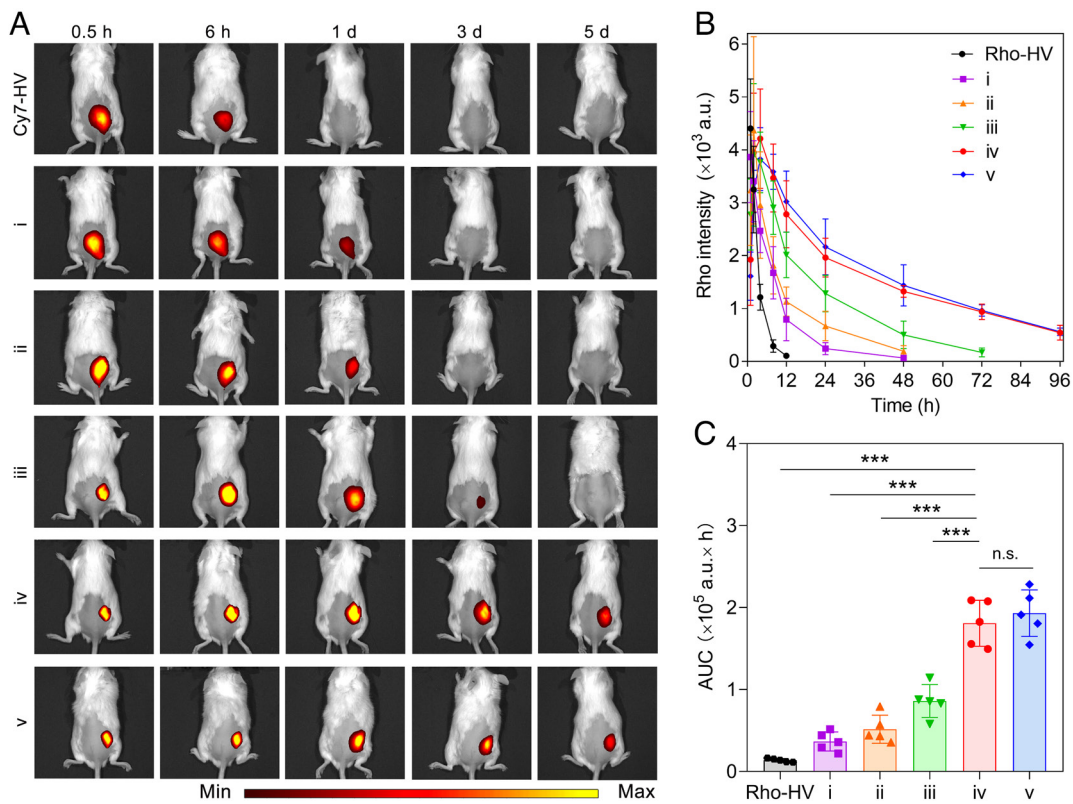


Fig. 3. In vivo retention and pharmacokinetic studies of ELPn-Fr-HVs with different lengths of ELP. (A) In vivo retention time of ELPn-Fr-HVs after subcutaneous injection. i: Cy7-ELP20-Fr-HV, ii: Cy7-ELP40-Fr-HV, iii: Cy7-ELP80-Fr-HV, iv: Cy7-ELP120-Fr-HV, v: Cy7-ELP160-Fr-HV. (B) Plasma Rho-ELPn-Fr-HVs levels versus time after subcutaneous injection and (C) the corresponding AUC. i: Rho-ELP20-Fr-HV, ii: Rho-ELP40-Fr-HV, iii: Rho-ELP80-Fr-HV, iv: Rho-ELP120-Fr-HV, v: Rho-ELP160-Fr-HV. Data are presented as the mean \pm SD, $n = 5$ independent animals. $P > 0.05$ (no significance, n.s.), *** $P < 0.001$.

injection. It is speculated that the in vivo phase transitions of Cy7-ELP120-Fr-HV and Cy7-ELP160-Fr-HV contribute to the formation of insoluble depots, which are slowly liberated to the circulatory system.

The pharmacokinetics of ELPn-Fr-HVs were further determined. Upon subcutaneous injection, Rho-HV was rapidly cleared from the body, while Rho-ELPn-Fr-HVs, especially Rho-ELP120-Fr-HV and Rho-ELP160-Fr-HV dropped much more slowly (Fig. 3B). The half-lives of Rho-ELP120-Fr-HV and Rho-ELP160-Fr-HV were 17.6- and 16.7-fold longer than that of Rho-HV, respectively (SI Appendix, Fig. S10). The area under the curves (AUCs) of Rho-ELP120-Fr-HV and Rho-ELP160-Fr-HV increased by 11.2 and 12.1 times compared to that of Rho-HV, respectively (Fig. 3C). Collectively, the extension of ELP repeat units generally leads to an increase in the retention time of the fusion proteins. There was no significant difference in either half-life or AUC between ELP120-Fr-HV and ELP160-Fr-HV, indicating that 120 repeat units have reached a plateau for long-term effect in vivo. Accordingly, ELP120-Fr-HV was selected for the following in vivo studies. The biodistribution of Cy7-ELP120-Fr-HV in the mice was further assessed. The mice receiving Cy7-ELP120-Fr-HV were killed on day 4 and day 7 after injection, and relevant organs and the tissue at the injection site were sampled for ex vivo fluorescence imaging. The results indicated that the fluorescent signals were detectable in the liver and kidneys on day 4, and gradually weakened on day 7 (SI Appendix, Fig. S11). By comparison, strong signals were visualized in the injection region within the studied time points.

In Vivo Anti-Clotting Efficacies. The long-term anticoagulant effect of ELP120-Fr-HV was first evaluated in the rat model of FeCl_3 -induced femoral arterial thrombosis (40). Various

treatments (saline, heparin, hirudin, ELP120-HV, and ELP120-Fr-HV) were injected subcutaneously into the back of rats. After different time intervals (2 h, 1 d, and 3 d), the left femoral arteries of rats were exposed and treated with FeCl_3 to induce vascular injury for thrombus formation (SI Appendix, Fig. S12A). MRI was used to monitor the blood flow signals of the vessels (Fig. 4A and SI Appendix, Fig. S13). In the saline and non-responsive ELP120-HV treatment groups, almost no blood flow signal in the FeCl_3 -treated region of the femoral arterial vessels was detected, which is indicative of blood clot formation. In the heparin and hirudin treatment groups, blood flow signals of the femoral arteries were strong at 2 h post administration but vanished on day 1 and day 3 after administration, suggesting the anticoagulation effects of heparin and hirudin are short-term. Notably, ELP120-Fr-HV exhibited sustained and potent anticoagulation efficacy, as evidenced by the steady blood flow signals at all the studied time points.

Furthermore, the rats were killed to sample femoral arteries for hematoxylin and eosin (H&E) and Masson's trichrome (MT)-stained histological examination (Fig. 4B). The injured vessels of rats treated with saline and ELP120-HV exhibited severe embolisms. Treatment with either hirudin or heparin efficiently inhibited thrombosis in a short time, while ELP120-Fr-HV provided prolonged inhibition, as evidenced by the low percentage of clot area as 1.8% at 2 h, 3.2% on day 1, and 20.3% on day 3 (Fig. 4C).

Next, the long-acting anti-clotting effect of ELP120-Fr-HV was estimated in the carotid arterial thrombosis mouse model (41). After receiving various treatments, the mice were injected with Rho 6G for platelet labeling, followed by the induction of carotid artery injury (SI Appendix, Fig. S12B). The clot degree of the mice was visualized using a fluorescent microscope and analyzed by Image

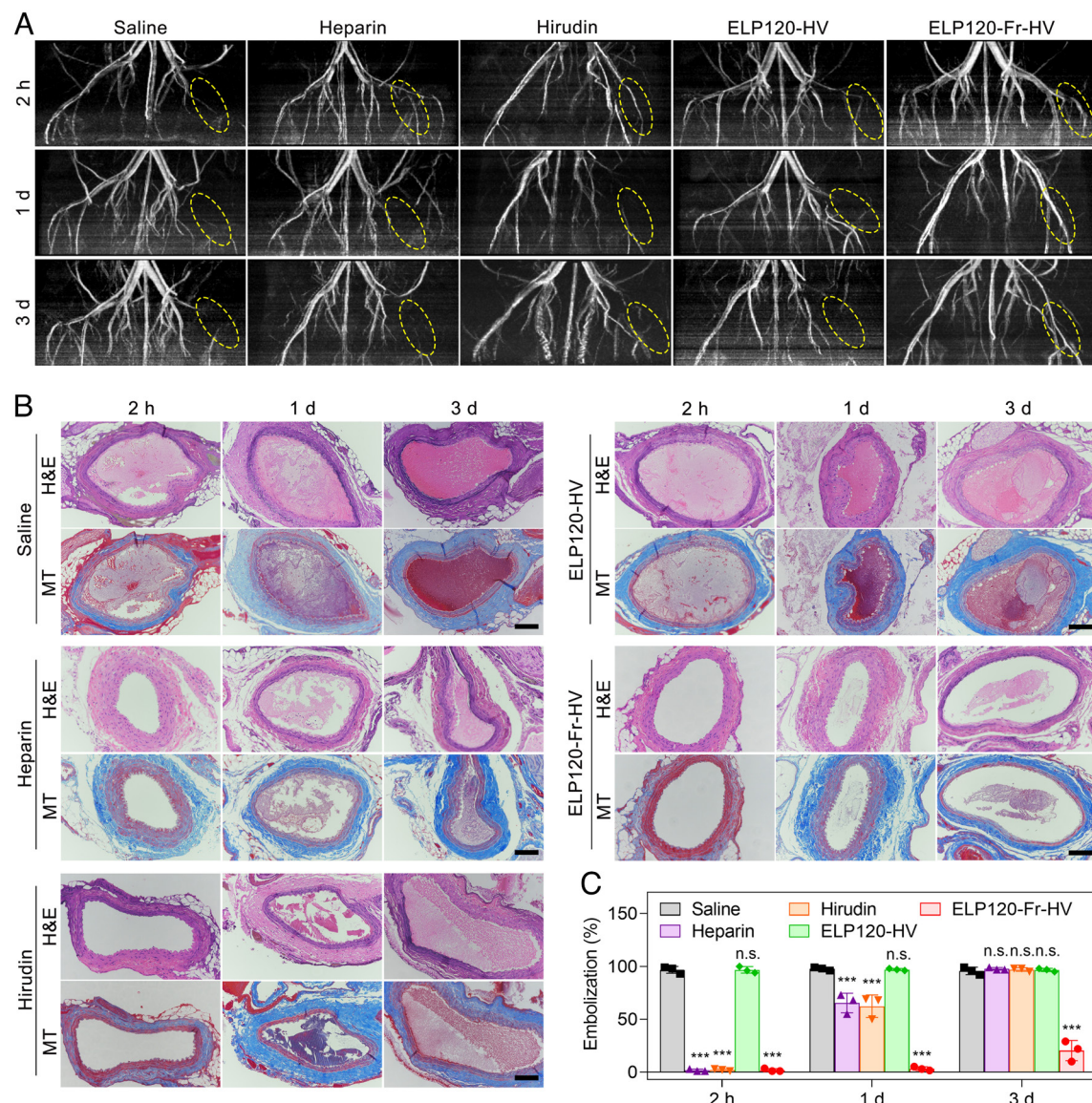


Fig. 4. In vivo anticoagulant effect in the rat model of FeCl_3 -induced femoral arterial thrombosis. (A) MRI of rats after different treatments. The yellow dashed line indicates the FeCl_3 -treated site. (B) H&E- and MT-stained images of the femoral arterial slices after various treatments. (Scale bar: 100 μm). (C) Embolization ratios of the H&E-stained femoral arterial slices in different treatment groups. Data are presented as the mean \pm SD, $n = 3$ independent animals. $P > 0.05$ (no significance, n.s.), *** $P < 0.001$ versus the saline group.

J software (Fig. 5 A and B). In the saline treatment group, the Rho fluorescence was sharply enhanced in the carotid arteries, indicating the formation of blood clots. Subcutaneous injection of heparin, hirudin, and ELP120-Fr-HV 2 h in advance all efficiently suppressed clot formation, as demonstrated by the negligible fluorescence of the FeCl_3 -treated region, while on day 1 and day 3 post administration, only the ELP120-Fr-HV treatment group maintained substantially weak fluorescent intensity. The sustained anti-clotting effect of ELP120-Fr-HV was reconfirmed by histological examinations that showed merely a small amount of thrombus in the injured vessels 3 d after treatment (Fig. 5 C and D).

The clot-inhibiting effect of ELP120-Fr-HV was further appraised in the pulmonary embolism mice (42). After the mice received different treatments, cyanine5.5-labeled fibrinogen and thromboplastin were injected into the tail vein in sequence to induce the formation of thrombus, which tends to deposit in capillary-rich lungs (*SI Appendix*, Fig. S12C). IVIS imaging of lung tissues showed that ELP120-Fr-HV produced a substantial

and lasting anti-pulmonary embolism effect, as evidenced by the notably low Cy5.5 intensity of fibrin deposition in the lung at all time points (Fig. 6 A and B). Histological examination of the lung sections showed that on day 3 post administration, ELP120-Fr-HV treatment led to the lowest level of pulmonary embolism, with a significant reduction in the percentage of embolism area to 26% of the saline treatment group (Fig. 6 C and D).

The survival of the thromboplastin-induced pulmonary embolism mice receiving different anticoagulants was also monitored. All the mice receiving ELP120-Fr-HV 3 d in advance survived the thromboplastin challenge (Fig. 6E). Moreover, we assessed the therapeutic efficacy of ELP120-Fr-HV using the repeated thromboplastin-induced pulmonary embolism mouse model (*SI Appendix*, Fig. S12D). The Cy5.5 intensity in the lung tissues remained weak after repeated thromboplastin challenges (Fig. 6F). Histological examinations showed that the degree of pulmonary embolism in lung tissues was low after repeated induction, which was comparable to that of a single induction (Fig. 6G and *SI Appendix*, Fig. S14).

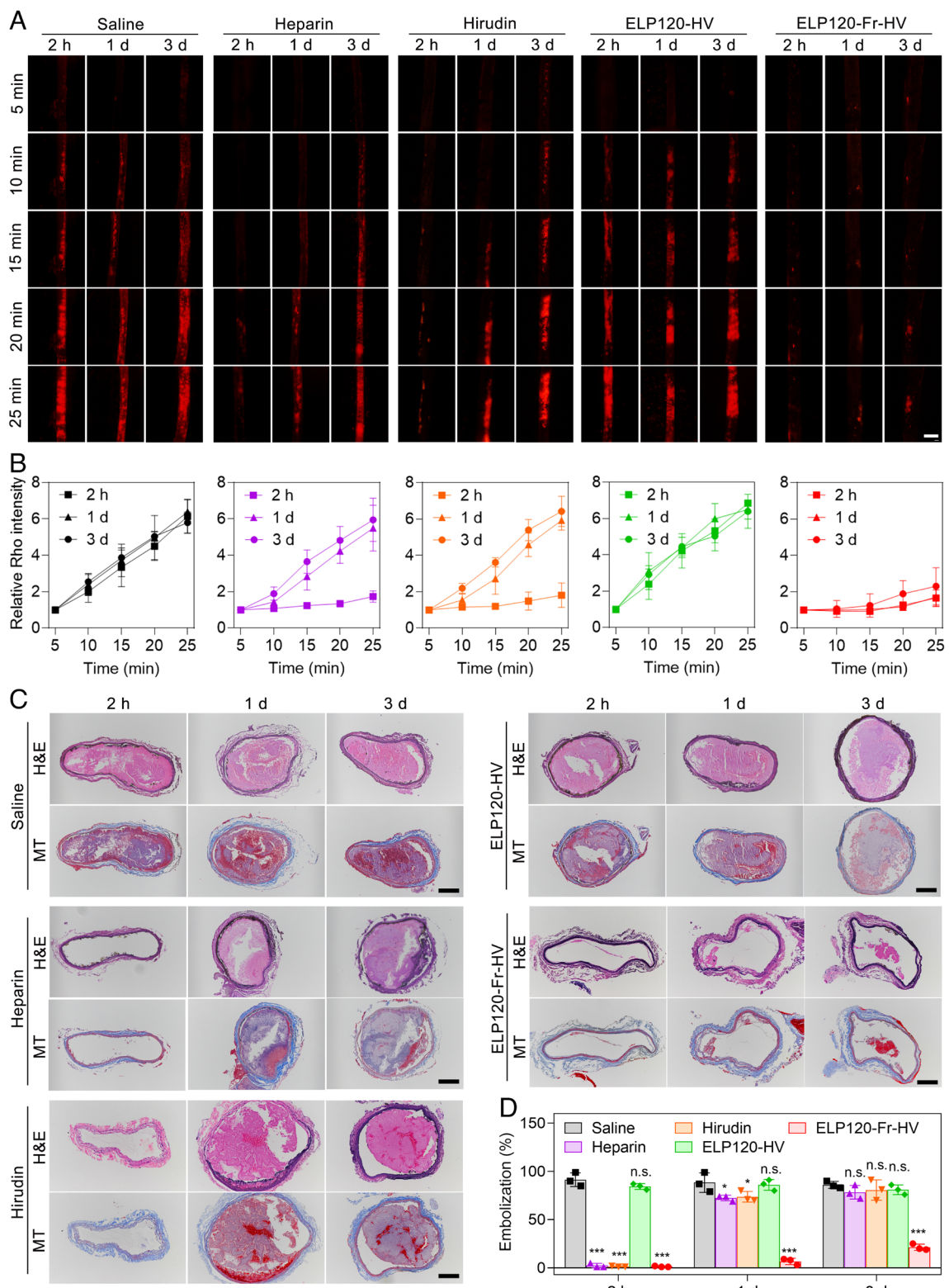


Fig. 5. In vivo anticoagulant effect in the mouse model of FeCl_3 -induced carotid arterial thrombosis. (A) Fluorescence photos of the carotid embolus of the mice after various treatments. (Scale bar: 500 μm .) (B) The fluorescent intensity variation of Rho versus time under various treatments. Data are presented as the mean \pm SD, $n = 3$ independent animals. (C) H&E- and MT-stained images of the carotid arterial slices. (Scale bar: 100 μm .) (D) Embolization ratios of the H&E-stained carotid arterial slices. Data are presented as the mean \pm SD, $n = 3$ independent animals. $P > 0.05$ (no significance, n.s.), $*P < 0.05$, $***P < 0.001$ versus the saline group.

Safety Evaluation. With the validation of long-term anti-clotting efficacies in different animal models, the safety assessments of ELP120-Fr-HV were performed. The in vitro hemolysis test was conducted by incubating red blood cells with ELP120-Fr-HV over time and detecting the absorbance of hemoglobin in the

supernatant after centrifugation. In contrast to the high absorbance value of the positive control, Triton X-100 treated group, the absorbance of saline and ELP120-Fr-HV group was very low and had no significant difference, indicating that ELP120-Fr-HV does not induce any hemolytic symptom (*SI Appendix*, Fig. S15).

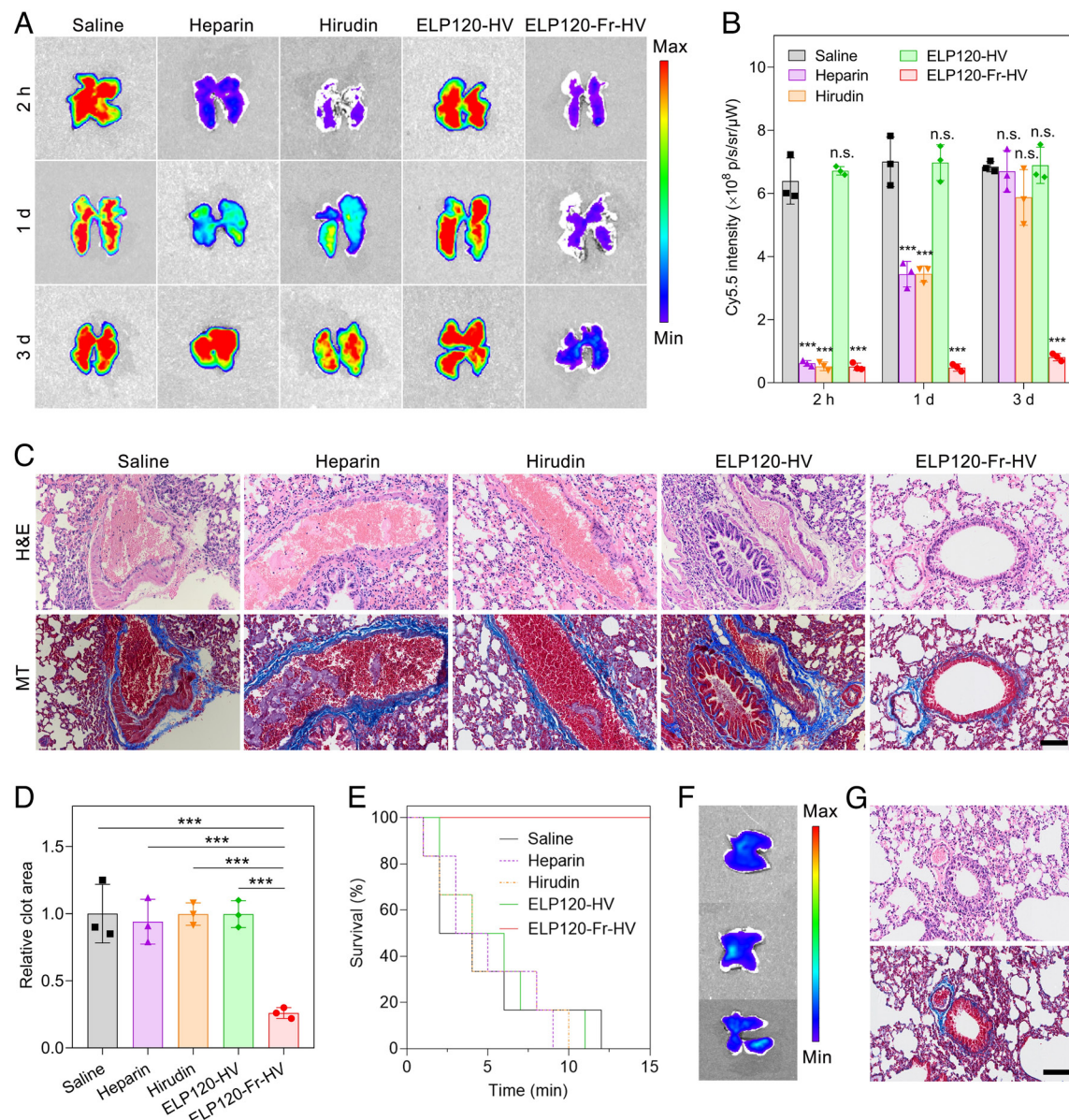


Fig. 6. In vivo antithrombotic study in the mouse model of pulmonary embolism. (A) Fluorescence photos and (B) quantitative study of Cy5.5 intensity of pulmonary embolism in mice receiving various treatments. Data are presented as the mean \pm SD, $n = 3$ independent animals. $P > 0.05$ (no significance, n.s.), *** $P < 0.001$ versus the saline group. (C) H&E- and MT-stained images of the lung slices of mice on day 3 post subcutaneous injection of various treatments. (Scale bar: 100 μ m.) (D) Relative clot area in the H&E-stained lung slices after various treatments. Data are presented as the mean \pm SD, $n = 3$ independent animals. *** $P < 0.001$. (E) Survival curves of the mice challenged with thromboplastin on day 3 post subcutaneous injection of various treatments. Six mice per treatment group. (F) Fluorescence photos of the lung tissues and (G) H&E (Upper)- and MT (Lower)-stained images of the lung sections sampled from the mice challenged with multiple times of thromboplastin induction on day 3 post administration of ELP120-Fr-HV. (Scale bar: 100 μ m.)

Bleeding risk is a common side effect associated with the clinical use of heparin and hirudin. To assess whether subcutaneous injection of ELP120-Fr-HV in high dose affected the hemostatic capability of the blood coagulation system, the bleeding time was monitored after different treatments. Treatment with both heparin and hirudin caused increased bleeding time, while ELP120-Fr-HV did not induce a noticeable change compared to the saline treatment group (*SI Appendix*, Fig. S16A).

In addition, the total amounts of platelets in mice were evaluated by a hematology analyzer. In comparison with a significant drop in platelet count caused by the heparin treatment, the ELP120-Fr-HV treatment did not induce any significant change (*SI Appendix*, Fig. S16B). Furthermore, ELP120-Fr-HV did not lead to any noticeable variation in the serum levels of biochemical parameters of the liver and kidney function (*SI Appendix*, Fig. S17),

as well as visible pathological changes in H&E staining sections of main organs (*SI Appendix*, Fig. S18).

Discussion

To achieve a long-acting and safe antithrombotic treatment strategy, we engineered a fusion protein consisting of hirudin, ELP, and responsive moiety using genetic engineering technology, which exhibited *in situ* depot formation, adjustable *in vivo* retention, and controlled bioactive recovery features. First, the developed Ffu312 tag was used to achieve efficient secretory expression of various passenger proteins at the yield of ~300 mg/L in the shake flask cultures. The secretory expression not only avoided protein degradation in the expression host but also simplified downstream separation operations. The fusion proteins were

purified by the facile ITC method benefiting from the reversible phase transition property of ELP, which eliminated the need for column chromatography. We found that the fusion order had a distinctive impact on the bioactivity of hirudin, as ELP-HV almost lost antithrombin activity while HV-ELP maintained bioactivity. Tetrapeptide IEGR as an FXa-degradable motif was introduced into the hirudin and ELP to obtain ELP-Fr-HV. Under the specific action of FXa, the biological activity of fusion protein ELP-Fr-HV underwent an off-on conversion, showing the prodrug-like feature.

Furthermore, we tailored a series of fusion proteins with different numbers of ELP repeat units and screened ELP120-Fr-HV as the study formulation. In various animal models, ELP120-Fr-HV has demonstrated its long-term effect on preventing and inhibiting thrombosis and embolism. Moreover, the safety evaluation showed that ELP120-Fr-HV did not induce any hemolytic reaction, thrombocytopenia or damage to liver and renal function within the studied period. Prior to the clinical translation of the fusion protein, a comprehensive assessment of the in vivo behaviors, such as metabolism, excretion, and biosafety should be conducted. The antithrombotic efficiency also needs to be further substantiated in large animal models.

PEG derivatization is a commonly used long-term strategy for protein and peptide therapeutics but has the limitations of non-specific chemical conjugation and low conjugation efficiency. By comparison, the ELP fusion proteins produced by genetic engineering techniques enable precise control over molecular

weight and modification site. The ELP fusion proteins with reservoir-like characteristics offer the merits of simple synthesis, easy purification, and homogeneous products. This in situ formed depot of the fusion protein can further load or conjugate with different therapeutics for treating various diseases in a long-term and bioresponsive manner (43, 44).

Materials and Methods

The *Escherichia coli* strain BL21(DE3) was purchased from Innovagen. The pET-22b(+) vector was obtained from Takara. Hirudin cDNA (genebank accession no. AAF85971.1) was synthesized by GenScrip Biotech. The Ffu312 tag was preserved in the lab (30). Detailed experimental procedures for *Plasmid Construction, Expression and Purification of Fusion Proteins, Antithrombin Assay, Phase Transition Characterizations, In Vitro Release, In Vivo Retention, Pharmacokinetics, In Vivo Therapeutic Efficacies, and Safety Assessments* are provided in *SI Appendix*.

Statistical Analysis. GraphPad Prism 8.0 was used for the statistical analysis. All the results are indicated as mean \pm SD. Two-tailed Student's *t* test and one-way ANOVA were applied for the statistical comparison in two and multiple groups, respectively.

Data, Materials, and Software Availability. All study data are included in the article and/or *SI Appendix*.

ACKNOWLEDGMENTS. This work was supported by the National Key Research and Development Program of China (2019YFA0905200) and the National Natural Science Foundation of China (82072045).

1. S. S. Virani *et al.*, Heart disease and stroke statistics-2021 Update A report from the American Heart Association. *Circulation* **143**, e254–e743 (2021).
2. W. Chen, J. Thomas, M. Sadatsafavi, J. M. FitzGerald, Risk of cardiovascular comorbidity in patients with chronic obstructive pulmonary disease: A systematic review and meta-analysis. *Lancet Respir. Med.* **3**, 631–639 (2015).
3. T. Boeckh-Behrens *et al.*, Thrombus histology suggests cardioembolic cause in cryptogenic stroke. *Stroke* **47**, 1864–1871 (2016).
4. N. Mackman, Triggers, targets and treatments for thrombosis. *Nature* **451**, 914–918 (2008).
5. S. S. Jolly *et al.*, Thrombus aspiration in ST-segment-elevation myocardial infarction: An individual patient meta-analysis: Thrombectomy trials collaboration. *Circulation* **135**, 143–152 (2017).
6. A. S. Wolberg *et al.*, Venous thrombosis. *Nat. Rev. Dis. Primers.* **1**, 150006 (2015).
7. F. Khan, T. Tritschler, S. R. Kahn, M. A. Rodger, Venous thromboembolism. *Lancet (London, England)* **398**, 64–77 (2021).
8. B. Furie, B. C. Furie, Mechanisms of disease: Mechanisms of thrombus formation. *New Engl. J. Med.* **359**, 938–949 (2008).
9. J. A. Heit, Epidemiology of venous thromboembolism. *Nat. Rev. Cardio.* **12**, 464–474 (2015).
10. H. Kamel, J. S. Healey, Cardioembolic stroke. *Circ. Res.* **120**, 514–526 (2017).
11. F. Crea, P. Libby, Acute coronary syndromes the way forward from mechanisms to precision treatment. *Circulation* **136**, 1155–1166 (2017).
12. T. Tritschler, N. Kraaijpoel, G. Le Gal, P. S. Wells, Venous thromboembolism advances in diagnosis and treatment. *JAMA* **320**, 1583–1594 (2018).
13. N. Mackman, W. Bergmeier, G. A. Stouffer, J. I. Weitz, Therapeutic strategies for thrombosis: New targets and approaches. *Nat. Rev. Drug Discov.* **19**, 333–352 (2020).
14. J. C. Fredenburgh, P. L. Gross, J. I. Weitz, Emerging anticoagulant strategies. *Blood* **129**, 147–154 (2017).
15. A. Greinacher, Heparin-induced thrombocytopenia. *New Engl. J. Med.* **373**, 252–261 (2015).
16. B. S. Salter *et al.*, Heparin-induced thrombocytopenia a comprehensive clinical review. *J. Am. Coll. Cardiol.* **67**, 2519–2532 (2016).
17. G. M. Arepally, Heparin-induced thrombocytopenia. *Blood* **129**, 2864–2872 (2017).
18. F. Markwardt, The development of hirudin as an antithrombotic drug. *Thromb. Res.* **74**, 1–23 (1994).
19. A. Greinacher *et al.*, Recombinant hirudin (lepirudin) provides safe and effective anticoagulation in patients with heparin-induced thrombocytopenia: A prospective study. *Circulation* **99**, 73–80 (1999).
20. T. J. Graetz, B. R. Tellor, J. R. Smith, M. S. Avidan, Desirudin: A review of the pharmacology and clinical application for the prevention of deep vein thrombosis. *Expert Rev. Cardiovasc. Ther.* **9**, 1101–1109 (2011).
21. D. W. Urry, Physical chemistry of biological free energy transduction as demonstrated by elastic protein-based polymers. *J. Phys. Chem. B* **101**, 11007–11028 (1997).
22. E. E. Fletcher, D. Yan, A. A. Kosiba, Y. Zhou, H. Shi, Biotechnological applications of elastin-like polypeptides and the inverse transition cycle in the pharmaceutical industry. *Protein Expr. Purif.* **153**, 114–120 (2019).
23. D. L. Nettles, A. Chilkoti, L. A. Setton, Applications of elastin-like polypeptides in tissue engineering. *Adv. Drug. Deliv. Rev.* **62**, 1479–1485 (2010).
24. S. R. Ong *et al.*, Epitope tagging for tracking elastin-like polypeptides. *Biomaterials* **27**, 1930–1935 (2006).
25. Z. Wang *et al.*, Thermoresponsive and protease-cleavable interferon-polypeptide conjugates with spatiotemporally programmed two-step release kinetics for tumor therapy. *Adv. Sci.* **6**, 1900586 (2019).
26. P. Liang *et al.*, Spatiotemporal combination of thermosensitive polypeptide fused interferon and temozolamide for post-surgical glioblastoma immunochemotherapy. *Biomaterials* **264**, 120447 (2021).
27. A. S. Wolberg, Thrombin generation and fibrin clot structure. *Blood Rev.* **21**, 131–142 (2007).
28. R. M. Bertina, Elevated clotting factor levels and venous thrombosis. *Pathophysiol. Haemost. Thromb.* **33**, 395–400 (2003).
29. Y. Zhang *et al.*, Thrombin-responsive cutaneous patch for auto-anticoagulant regulation. *Adv. Mater.* **29**, 1604043 (2017).
30. M. F. Maitz *et al.*, Bio-responsive polymer hydrogels homeostatically regulate blood coagulation. *Nat. Commun.* **4**, 2168 (2013).
31. X. Xu *et al.*, Self-regulated hirudin delivery for anticoagulant therapy. *Sci. Adv.* **6**, eabc0382 (2020).
32. M. F. Maitz *et al.*, Adaptive release of heparin from anticoagulant hydrogels triggered by different blood coagulation factors. *Biomaterials* **135**, 53–61 (2017).
33. C. Cheng *et al.*, A novel Ffu fusion system for secretory expression of heterologous proteins in *Escherichia coli*. *Microb. Cell Fact.* **16**, 231 (2017).
34. L. Cui, C. Cheng, Y. Qiu, T. Jiang, B. He, Excretory overexpression of hydrophobins as multifunctional biosurfactants in *E. coli*. *Int. J. Biol. Macromol.* **165**, 1296–1302 (2020).
35. D. E. Meyer, A. Chilkoti, Purification of recombinant proteins by fusion with thermally-responsive polypeptides. *Nat. Biotechnol.* **17**, 1112–1115 (1999).
36. A. Betz, J. Hofsteenge, S. R. Stone, Interaction of the N-terminal region of hirudin with the active-site clef of thrombin. *Biochemistry* **31**, 4557–4562 (1992).
37. B. I. Ratnikov *et al.*, Basis for substrate recognition and distinction by matrix metalloproteinases. *Proc. Natl. Acad. Sci. U.S.A.* **111**, E4148–E4155 (2014).
38. B. M. Dunn, S. H. Hung, The two sides of enzyme-substrate specificity: Lessons from the aspartic proteinases. *Biochim. Biophys. Acta* **1477**, 231–240 (2000).
39. L. Hedstrom, Serine protease mechanism and specificity. *Chem. Rev.* **102**, 4501–4523 (2002).
40. F. Zhang *et al.*, Metal-organic-framework-derived carbon nanostructures for site-specific dual-modality photothermal/photodynamic thrombus therapy. *Adv. Sci.* **6**, 1901378 (2019).
41. L. Musumeci *et al.*, Dual-specificity phosphatase 3 deficiency or inhibition limits platelet activation and arterial thrombosis. *Circulation* **131**, 656–658 (2015).
42. E. J. Weiss, J. R. Hamilton, K. E. Lease, S. R. Coughlin, Protection against thrombosis in mice lacking PAR3. *Blood* **100**, 3240–3244 (2002).
43. Y. Lu, A. A. Aimetti, R. Langer, Z. Gu, Bioresponsive materials. *Nat. Rev. Mater.* **2**, 16075 (2017).
44. J. Zhang *et al.*, Week-long norm glycaemia in diabetic mice and minipigs via a subcutaneous dose of a glucose-responsive insulin complex. *Nat. Biomed. Eng.* 10.1038/s41515-023-01138-7 (2023), in press.